Filtered Tractography: State estimation in a constrained subspace

James G. Malcolm Martha E. Shenton Yogesh Rathi

Psychiatry Neuroimaging Laboratory, Harvard Medical School, Boston, MA
VA Boston Healthcare System, Brockton Division, Brockton, MA

Abstract. We describe a method of deterministic tractography using model-based estimation that remains constrained to the subspace of valid tensor mixture models. Existing techniques estimate the local fiber orientation at each voxel independently so there is no running knowledge of confidence in the estimated fiber model. We formulate fiber tracking as recursive estimation: at each step of tracing the fiber, the current estimate is guided by the previous. To do this we model the signal as a weighted mixture of Gaussian tensors and perform tractography within a filter framework. Starting from a seed point, each fiber is traced to its termination using an unscented Kalman filter to simultaneously fit the local model and propagate in the most consistent direction. Further, we modify the Kalman filter to enforce model constraints, *i.e.* positive eigenvalues and convex weights, thereby constraining it to a subspace of allowable model parameters. Despite the presence of noise and uncertainty, this provides a causal estimate of the local structure at each point along the fiber. Synthetic experiments demonstrate that this approach significantly improves the angular resolution at crossings and branchings while consistently estimating the mixture weights. *In vivo* experiments confirm the ability to trace out fibers in areas known to contain such crossing and branching while providing inherent path regularization. We conclude by applying unsupervised clustering to provide side-by-side comparison of the models.

1 Introduction

The advent of diffusion weighted magnetic resonance imaging has provided the opportunity for non-invasive investigation of neural architecture. Using this imaging technique, neuroscientists can investigate how neurons originating from one region connect to other regions, or how well-defined these connections may be. For such studies, the quality of the results relies heavily on the chosen fiber representation and the method of reconstructing pathways.

To begin studying the microstructure of fibers, we need a model to interpret the diffusion weighted signal. Such models fall broadly into two categories: parametric and nonparametric. One of the simplest parametric models is the diffusion tensor which describes a Gaussian estimate of the diffusion orientation and strength at each voxel. While robust, this model can be inadequate in cases of mixed fiber presence or more complex orientations, and so to handle more complex diffusion patterns, various alternatives have been introduced: weighted mixtures [1,2,3,4], higher order tensors [5], and directional functions [6]. In contrast, nonparametric techniques estimate an orientation distribution function (ODF) describing an arbitrary configuration of fibers. For

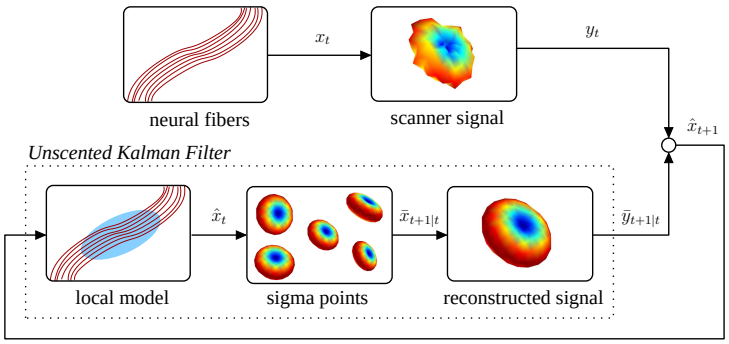

Fig. 1: System overview illustrating relation between the neural fibers, the scanner signal, and the unscented Kalman filter as it is used to estimate the local model. At each step, the filter uses its current model state to reconstruct a synthetic signal and then compares that against the actual signal from the scanner in order to update its internal model state.

this estimation, several techniques have been proposed, among them Q-ball imaging [2], spherical harmonics [7,8], spherical deconvolution [9,10,11,6], and diffusion orientation transforms [12].

Based on these models, several techniques can be used to reconstruct pathways. Deterministic tractography using the single tensor model simply follows the principal diffusion direction, while multi-fiber models use various techniques for determining the number of fibers present or when pathways branch [3,13]. While parametric methods directly describe the principal diffusion directions, interpreting the ODFs from model independent representations typically involves a separate algorithm to determine the number and orientation of diffusion patterns present [14,9,8,15]. Several filtering approaches have been proposed. For example, Kalman and particle filters [16,17,18], as well as a moving least squares approach [19], have been used with single tensor streamline tractography, but these have been used for path regularization and not to estimate the underlying fiber model. One approach has used a linear Kalman filter, although this method was applied to estimate each voxel independently during acquisition [20].

1.1 Our contributions

Of the approaches listed above, nearly all fit the model at each voxel independent of other voxels; however, tractography is a causal process: we arrive at each new position along the fiber based upon the diffusion found at the previous position. In this paper, we treat model estimation and tractography as such by placing this process within a causal filter. As we examine the signal at each new position, the filter recursively updates the underlying local model parameters, provides the variance of that estimate, and indicates the direction in which to propagate tractography.

To begin estimating within a finite dimensional filter, we model the diffusion signal using a weighted mixture of two tensors. This enables estimation directly from the raw signal without separate preprocessing or regularization. Because the signal reconstruction is nonlinear, we use the unscented Kalman filter to perform local model estimation and then propagate in the most consistent direction (Fig. 1). Further, we use a constrained version of the unscented Kalman filter to ensure the tensor eigenvalues are positive and the mixture weights are non-negative and convex. Using causal estimation

in this way yields inherent path regularization, consistent partial volume estimation, and accurate fiber resolution at crossing angles not found with independent optimization.

2 Approach

The main idea of our approach is to trace the local fiber orientations using the estimation at previous positions to guide estimation at the current position. In a loop, the Kalman filter estimates the model at the current position, moves a step in that direction, and then begins estimation again. Recursive estimation in this manner greatly improves the accuracy of resolving individual orientations and yields inherently smooth tracts despite the presence of noise and uncertainty.

Section 2.1 provides the necessary background on modeling the measurement signal using tensors and defines the specific weighted two-fiber model employed in this study. Then, Section 2.2 describes how this model can be estimated using an unscented Kalman filter and further how the constraints are enforced.

2.1 Modeling local fiber orientations

In diffusion weighted imaging, image contrast is related to the strength of water diffusion, and our goal is to accurately relate these signals to an underlying model of putative fibers. At each image voxel, diffusion is measured along a set of distinct gradients, $\mathbf{u}_1, ..., \mathbf{u}_m \in \mathbb{S}^2$ (on the unit sphere), producing the corresponding signal, $\mathbf{s} = [\, s_1, ..., s_m \,]^T \in \mathbb{R}^m$. For voxels containing a mixed diffusion pattern, a general weighted formulation is expressed as, $s_i = s_0 \sum_j w_j e^{-b\mathbf{u}_i^T D_j \mathbf{u}_i}$, where s_0 is the baseline signal intensity, b is an acquisition-specific constant, w_j are convex weights, and D_j are tensors, each representing a diffusion pattern.

From that general mixture model, we choose a restricted form with only two weighted components. This choice is guided by several previous studies which found two-component models to be sufficient at $b = 1000$ [2,3,13,14,4,21]. Also, we assume the shape of each tensor to be ellipsoidal, *i.e.* there is one dominant principal diffusion direction $\mathbf{m}$ with eigenvalue λ_1 and the remaining orthonormal directions have equal eigenvalues $\lambda_2 = \lambda_3$ (as in [4,6]). These assumptions leave us with the following model used in this study:

$$s_i = s_0 w_1 e^{-b\mathbf{u}_i^T D_1 \mathbf{u}_i} + s_0 w_2 e^{-b\mathbf{u}_i^T D_2 \mathbf{u}_i}, \tag{1}$$

where w_1, w_2 are convex weights and D_1, D_2 are each expressible as $D = \lambda_1 \mathbf{m}\mathbf{m}^T + \lambda_2 \left(\mathbf{p}\mathbf{p}^T + \mathbf{q}\mathbf{q}^T\right)$, with $\mathbf{m}, \mathbf{p}, \mathbf{q} \in \mathbb{S}^2$ forming an orthonormal basis aligned to the principal diffusion direction $\mathbf{m}$. The free model parameters are then $\mathbf{m}_1$, λ_{11}, λ_{21}, w_1, $\mathbf{m}_2$, λ_{12}, λ_{22}, and w_2. Lastly, we wish to constrain this model to have positive eigenvalues and convex weights ($w_1, w_2 \geq 0$ and $w_1 + w_2 = 1$).

2.2 Estimating the fiber model

Given the measured signal at a particular voxel, we want to estimate the underlying model parameters that explain this signal. As in streamline tractography, we treat the fiber as the trajectory of a particle which we trace out. At each step, we examine the measured signal at that position, use that measurement to update our model parameters within the filter, and propagate forward in the most consistent direction. Fig. 1 illustrates this filtering process.

Algorithm 1 Unscented Kalman Filter

1: Form weighted sigma points $\mathbf{X}_t = \{w_i, \mathbf{x}_i\}_{i=0}^{2n}$ around current mean $\mathbf{x}_t$ and covariance P_t with scaling factor ζ

$$\mathbf{x}_0 = \mathbf{x}_t \qquad \mathbf{x}_i = \mathbf{x}_t + [\sqrt{\zeta P_t}]_i \qquad \mathbf{x}_{i+n} = \mathbf{x}_t - [\sqrt{\zeta P_t}]_i$$

2: Predict the new sigma points and observations

$$\mathbf{X}_{t+1|t} = f[\mathbf{X}_t] \qquad \mathbf{Y}_{t+1|t} = h[\mathbf{X}_{t+1|t}]$$

3: Compute weighted means and covariances, *e.g.*

$$\bar{\mathbf{x}}_{t+1|t} = \sum_i w_i\, \mathbf{x}_i \qquad P_{xy} = \sum_i w_i (\mathbf{x}_i - \bar{\mathbf{x}}_{t+1|t})(\mathbf{y}_i - \bar{\mathbf{y}}_{t+1|t})^T$$

4: Update estimate using Kalman gain K and scanner measurement $\mathbf{y}_t$

$$\mathbf{x}_{t+1} = \bar{\mathbf{x}}_{t+1|t} + K(\mathbf{y}_t - \bar{\mathbf{y}}_{t+1|t}) \qquad P_{t+1} = P_{xx} - K P_{yy} K^T \qquad K = P_{xy} P_{yy}^{-1}$$

To use a state-space filter for estimating the model parameters, we need the application-specific definition of four filter components:

1. The system state ($\mathbf{x}$): the model parameters
2. The state transition function (f): how the model changes as we trace the fiber
3. The observation function (h): how the signal appears given a particular model state
4. The measurement ($\mathbf{y}$): the actual signal obtained from the scanner

For our state, we directly use the parameters for the two-tensor model in Eq. 1:

$$\mathbf{x} = [\,\mathbf{m}_1 \;\; \lambda_{11} \;\; \lambda_{21} \;\; w_1 \;\; \mathbf{m}_2 \;\; \lambda_{12} \;\; \lambda_{22} \;\; w_2\,]^T, \quad \mathbf{m} \in \mathbb{S}^2, \lambda \in \mathbb{R}^+, w \in [0,1]. \tag{2}$$

For the state transition we assume identity dynamics; the local fiber configuration does not undergo drastic change as it moves from one location to the next. Our observation is the signal reconstruction, $\mathbf{y} = h[\mathbf{x}] = \mathbf{s} = [\,s_1, ..., s_m\,]^T$ using s_i described by the model in Eq. 1, and our measurement is the actual signal interpolated directly on the diffusion weighted images at the current position.

Since our signal reconstruction in Eq. 1 is nonlinear, we employ an unscented Kalman filter to perform estimation. Similar to classical linear Kalman filtering, the unscented version seeks to reconcile the predicted state of the system with the measured state and addresses the fact that these two processes–prediction and measurement–may be non-linear or unknown. In Algorithm 1 we present the standard version of this filter; for more thorough treatments, see [22,23]. It is important to note that while particle filters are a common approach to nonlinear estimation, we chose instead the unscented Kalman filter primarily for its low computational complexity. With respect to state dimension, particle filters require the number of particles to be exponential to properly explore the state space. In contrast, the unscented filter requires $2n + 1$ particles (sigma points) for a Gaussian estimate of the n-dimensional state.

In this standard formulation, we have ignored the constraints on our model. This results in instabilities: the diffusion tensors may become degenerate with zero or negative eigenvalues, or the weights may become negative. To enforce appropriate constraints, one can directly project any unconstrained state $\mathbf{x}$ onto the constrained subspace [23]. In other words, we wish to find the state $\hat{\mathbf{x}}$ closest to the unconstrained state $\mathbf{x}$ which still obeys the constraints, $A\hat{\mathbf{x}} \leq \mathbf{b}$. Using P_t as a weighting matrix, this becomes a

quadratic programming problem:

$$\min_{\hat{\mathbf{x}}} (\mathbf{x} - \hat{\mathbf{x}})^T P_t^{-1} (\mathbf{x} - \hat{\mathbf{x}}) \quad \text{subject to} \quad A\hat{\mathbf{x}} \leq \mathbf{b}. \tag{3}$$

This projection procedure is applied within unscented Kalman filter procedure to correct at every place where we move in the state-space: after spreading the sigma points $\mathbf{X}_t$, after transforming the sigma points $\mathbf{X}_{t+1|t}$, and after the final estimate $\mathbf{x}_{t+1}$.

In this study, for voxels that can be modeled with only one tensor, we found it preferable to have both the tensor components similarly oriented. Upon encountering a region of dispersion, the second component is poised and ready to begin branching instead of having zero weight and arbitrary orientation. To favor such solutions, we require the weights of each of the components to be not just non-negative but also greater than 0.2, and so, in our current implementation, A and $\mathbf{b}$ are constructed to encode the following state constraints:

$$\lambda_{1_1}, \lambda_{2_1}, \lambda_{1_2}, \lambda_{2_2} > 0 \qquad w_1, w_2 \geq 0.2 \qquad w_1 + w_2 = 1. \tag{4}$$

3 Experiments

We first use experiments with synthetic data to validate our technique against ground truth. We confirm that our approach accurately recognizes crossing fibers over a broad range of angles and consistently estimates the partial volumes (Section 3.1). We then examine a real dataset to demonstrate how causal estimation is able to pick up fibers and branchings known to exist *in vivo* yet absent using other techniques (Section 3.2). Last, we use unsupervised clustering of single- and two-tensor tractography to highlight differences (Section 3.3).

In these experiments, we compare against two alternative techniques. First, we use sharpened spherical harmonics with peak detection as described in [8] (order $l = 8$, regularization $L = 0.006$). This provides a comparison with an independently estimated nonparametric representation. Second, when performing tractography on real data, we also compare against single-tensor streamline tractography for a baseline.

3.1 Synthetic validation

Following the experimental method of generating multi-compartment synthetic data found in [2,8,15], we averaged the eigenvalues of the 300 voxels with highest fractional anisotropy (FA) in our real data set: $\{1200, 100, 100\}\mu$m^2/msec. We used these eigenvalues to generate synthetic MR signals according to Eq. 1 at $b = 1000$ with 81 gradient directions on the hemisphere and introduced Rician noise (SNR $\approx$ 5 dB).

While the independent optimization techniques can be run on individually generated voxels, care must be taken in constructing reasonable scenarios to test the causal filter. For this purpose, we constructed a set of two-dimensional fields through which to navigate. In the middle is one long pathway where the filter starts at one end estimating a single tensor but then runs into voxels with two crossed fibers at a fixed angle and weighting. In this crossing region we calculated error statistics to compare against sharpened spherical harmonics.

From these synthetic sets, we examined detection rate, angular resolution, and estimated volume fractions and we plot the results in Fig. 2. Each column looks at a different primary-secondary weighting combination, and each row looks at a different metric. In the top row, we count how many times each technique distinguishes two sep-

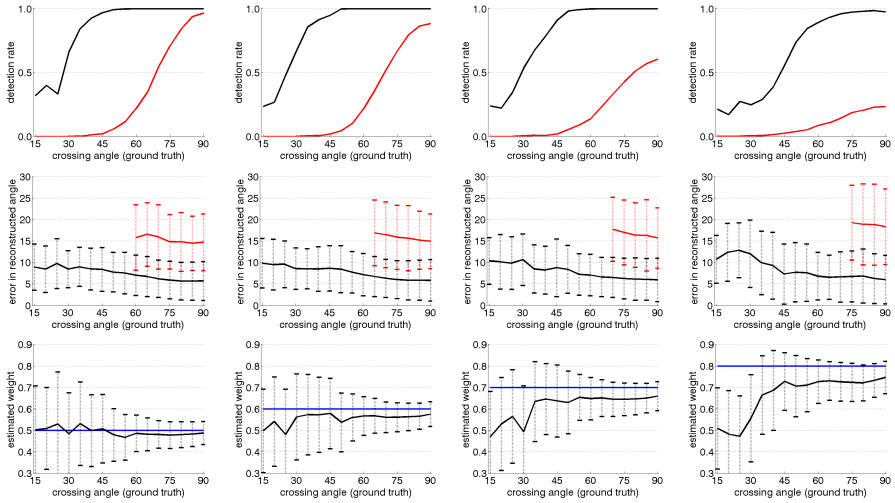

50%-50% 60%-40% 70%-30% 80%-20%

Fig. 2: Comparison of sharpened spherical harmonics *(red)* against filtered approach *(black)* over several different metrics: detection rate, angular resolution, estimated primary fiber weight *(rows, top to bottom)*. Each column is a different primary fiber weighting. The filter provides superior detection rates, accurate angular resolution, and consistent weight estimated. Trendlines indicate mean while dashed bars indicate one standard deviation.

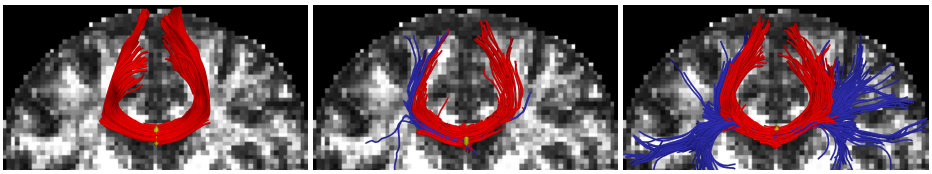

Single-tensor Spherical harmonics Filtered

Fig. 3: Filtered tractography picks up many fiber paths consistent with the underlying structures. Both single-tensor streamline and sharpened spherical harmonics are unable to find the majority of these pathways. Seed region indicated in yellow.

arate fibers. The filtered approach *(black)* is able to detect two distinct fibers at crossing angles far below that using spherical harmonics *(red)*. Further, the filtered approach maintains such relatively high detection rates even at 80/20 partial voluming *(far right column)*. In the middle row, we look at where each technique reported two fibers and we record the error in estimated angles. From this, we see that spherical harmonics result in an angular error of roughly 15° at best and fails to detect a second component at angles below 60°. In contrast, the filtered approach has an error between 5-10° and is able to accurately estimate down to crossing angles of 30°. In the bottom row, we look at the primary fiber weight estimated by the filter. As expected, this estimate is most accurate closer to 90° *(blue line indicates true weight)*.

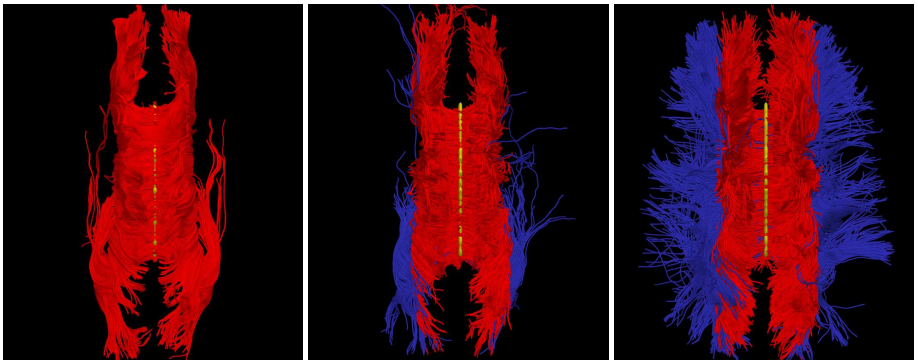

Single-tensor Spherical harmonics Filtered

Fig. 4: Tracing fibers originating from the center of the entire corpus callosum viewed from above. The proposed filtered tractography is able to find many of the lateral projections *(blue)* while single-tensor is unable to find any and few are found with sharpened spherical harmonics. Seed region indicated in yellow.

3.2 *In vivo* tractography

This study focuses on fibers originating in the corpus callosum. Specifically, we sought to trace out the lateral transcallosal fibers that run through the corpus callosum out to the lateral gyri. It is known that single-tensor streamline tractography only traces out the dominant pathways forming the U-shaped callosal radiation while spherical harmonics only capture some of these pathways [8,15].

We begin by seeding each algorithm up to thirty times in voxels at the intersection of the mid-sagital plane and the corpus callosum. To explore branchings found using the proposed technique, we considered a component to be branching if it was separated from the primary component by less than 40° with FA$\geq$0.15 and weight above 0.3. Similarly, with sharpened spherical harmonics, we considered it a branch if we found additional maxima over the same range. We terminated fibers when either the generalized fractional anisotropy [2] of the estimated signal fell below 0.1 or the primary component FA fell below 0.15 or weight below 0.3.

We tested our approach on a human brain scan using a 3-Tesla magnet to collect 51 diffusion weighted images on the hemisphere at $b = 900\,\mathrm{s/mm}^2$, a scan sequence comparable those of [8,15]. Fig. 3 shows tracts originating from within a few voxels intersecting a chosen coronal slice. Confirming the results in [8,15], sharpened spherical harmonics only pick up a few fibers intersecting the U-shaped callosal radiata. In contrast, our proposed algorithm traces out many pathways consistent with the apparent anatomy. Fig. 4 shows a view of the whole corpus callosum from above. The filtered approach is able to pick up many transcallosal fibers throughout the corpus callosum as well as infiltrating the frontal gyri to a greater degree than either alternate technique. To emphasize transcallosal tracts, we color as blue those fibers exiting a corridor of ± 22 mm around the mid-sagittal plane.

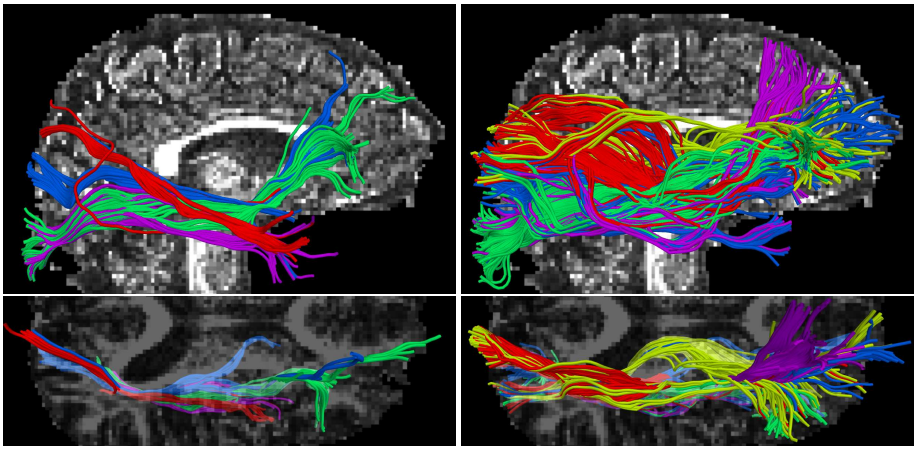

Single-tensor Two-tensor

Fig. 5: Clustering fronto-occipital fibers using both single- and two-tensor models. Using the same seed regions, the two-tensor model finds many more potential connections. Top row is a side view; bottom row is a top view.

3.3 Clustering

In a final set of experiments, we used unsupervised clustering of the single- and two-tensor tracts to provide side-by-side comparison between the two approaches. For clustering, we use affinity propagation [24]. Similar to spectral and hierarchical methods, affinity propagation takes as input a square affinity matrix defining the "distance" between any two fibers. In addition it requires a preference parameter which essentially defines the preferred cluster size. With these, it automatically determines the resulting number of clusters.

There are several key features of affinity propagation that make it an attractive choice in clustering fibers. First, the affinity matrix can be non-metric, so in this study we use the negative mean Chamfer distance itself and are able to avoid the extra unnecessary steps of symmetrizing the distance [25] and converting it to an inner product based on a radial-basis function requiring yet another bandwidth parameter [26]. Fig. 5 shows a clustering of fronto-occipital fibers in the right hemisphere using this approach. Visible in both techniques are false-positives; however, we believe that the increased density and crossing pathways of multi-tensor methods will require more precise distance measures than simply the Chamfer or Hausdorff measures. Fig. 6 examines a full clustering of the right hemisphere. We believe affinity propagation may provide natural cortical segmentations as seen when all the clusters for single-tensor tractography are combined. On the right, we select out several of the major two-tensor clusters to show their denser cortical insertions. One drawback to all unsupervised clustering algorithms is that they are oblivious to actual anatomy: here we see the upper and lower arcuate are separated into two clusters and merged with part of the uncinate.

A second property of affinity propagation is that cluster centers themselves are fibers. In contrast, methods such as k-means and expectation maximization find the cluster centers (called "exemplars") to be weighted combination of input fibers, a value

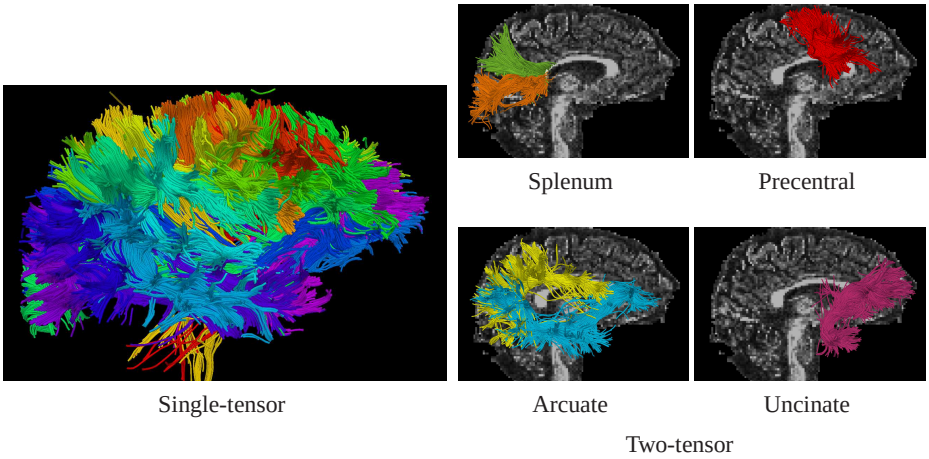

Fig. 6: Clustering of pathways in the right hemisphere. On the left, we view all of the single-tensor clusters together. On the right, we focus on several two-tensor clusters. Compared to the single-tensor clusters, the two-tensor clusters have denser cortical insertions.

which requires some basis for representation. Fig. 7 shows the cluster exemplars for the fronto-occipital pathways previously shown.

Third, the clustered solution is completely dependent on the distance measure and the preference parameter–no additional information is needed. For example, increasing this preference parameter produces a monotonically increasing number of clusters, essentially segmenting the anatomy at smaller and smaller scales. Further, this preference parameter is typically problem specific and often the mean affinity matrix value is chosen as a initial guess. Fig. 8 shows how a segmentation of the corpus callosum along the mid-sagittal plane is further parcellated as the preference parameter is increased. Two-tensor tractography shows increased segmentation due to the clustering of lateral branches seen in Fig. 4. The lack of correspondence between both methods on the same patient suggests that affinity propagation may not produce consistent clusters across a group of patients.

Last, affinity propagation does not require eigen-decomposition of the Gram matrix, but instead iteratively passes scalar values between points until a clustering emerges, an approach that allows it to scale to larger problem sizes infeasible with eigen-decomposition. In our experiments, we were able to segment 30,000 fiber tracts in about six hours using MATLAB. [1]

4 Conclusion

In this work, we demonstrated that using the unscented Kalman filter provides robust estimates of the fiber model with much higher accuracy than independent estimation techniques. Specifically, the proposed approach gives significantly lower angular error (5-10°) in regions with fiber crossings than using sharpened spherical harmonics (15-20°), and it reliably estimates the partial volume fractions.

[1] http://www.psi.toronto.edu/affinitypropagation

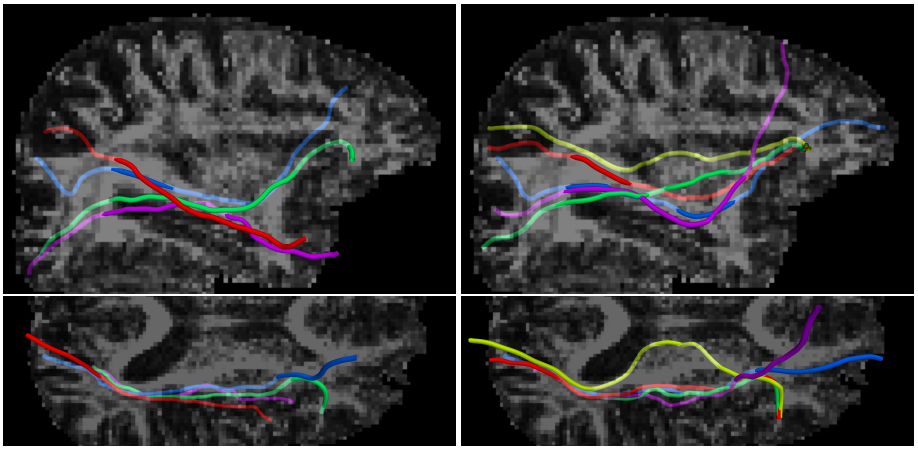

Single-tensor Two-tensor

Fig. 7: Exemplar fronto-occipital fibers underlying Fig. 5. Both models found essentially the same major cluster centers, and so the primary differences are in the many minor branches and insertions found using the two-tensor method.

Initial experiments using affinity propagation for unsupervised fiber clustering are promising; however, we believe if to be unsuitable for group analysis. As Fig. 8 shows, clustering can be highly dependent on preference parameter. By its nature (unsupervised) it is not obvious how to incorporate anatomical atlases to help guide clustering. It appears quite suitable for patient-specific studies such as cortical parcellation due to its relatively simple implementation and single parameter determining cluster size. Nevertheless, its use here was simply to provide side-by-side comparison between the single- and two-tensor tractography. In doing so, it revealed a need for suppressing false-positive connections, something we strongly believe will require more global information in the form of anatomical priors.

References

1. Alexander, A., Hasan, K., Tsuruda, J., Parker, D.: Analysis of partial volume effects in diffusion-tensor MRI. Magnetic Resonance in Medicine **45** (2001) 770–780
2. Tuch, D., Reese, T., Wiegell, M., Makris, N., Belliveau, J., Wedeen, V.: High angular resolution diffusion imaging reveals intravoxel white matter fiber heterogeneity. Magnetic Resonance in Medicine **48** (2002) 577–582
3. Kreher, B., Schneider, J., Mader, I., Martin, E., Hennig, J., Il'yasov, K.: Multitensor approach for analysis and tracking of complex fiber configurations. Magnetic Resonance in Medicine **54** (2005) 1216–1225
4. Peled, S., Friman, O., Jolesz, F., Westin, C.F.: Geometrically constrained two-tensor model for crossing tracts in DWI. Magnetic Resonance in Medicine **24**(9) (2006) 1263–1270
5. Basser, P., Pajevic, S.: Spectral decomposition of a 4th-order covariance tensor: Applications to diffusion tensor MRI. Signal Processing **87** (2007) 220–236
6. Kaden, E., Knøsche, T., Anwander, A.: Parametric spherical deconvolution: Inferring anatomical connectivity using diffusion MR imaging. NeuroImage **37** (2007) 474–488
7. Anderson, A.: Measurement of fiber orientation distributions using high angular resolution diffusion imaging. Magnetic Resonance in Medicine **54**(5) (2005) 1194–1206

Single-tensor

Two-tensor

Fig. 8: Clustering fibers passing through the corpus callosum provides a segmentation along the mid-sagittal plane. Varying the preference parameter in affinity propagation produces a range of segmentations at various scales. The lateral branches found in two-tensor tractography result in increased corpus segmentation.

8. Descoteaux, M., Deriche, R., Anwander, A.: Deterministic and probabilistic Q-ball tractography: from diffusion to sharp fiber distributions. Technical Report 6273, INRIA (2007)
9. Jian, B., Vemuri, B.: A unified computational framework for deconvolution to reconstruct multiple fibers from diffusion weighted MRI. IEEE Trans. on Med. Imag. **26**(11) (2007) 1464–1471
10. Jansons, K., Alexander, D.: Persistent angular structure: New insights from diffusion MRI data. Inverse Problems **19** (2003) 1031–1046
11. Tournier, J.D., Calamante, F., Gadian, D., Connelly, A.: Direct estimation of the fiber orientation density function from diffusion-weighted MRI data using spherical deconvolution. NeuroImage **23** (2004) 1176–1185
12. Özarslan, E., Shepherd, T., Vemuri, B., Blackband, S., Mareci, T.: Resolution of complex tissue microarchitecture using the diffusion orientation transform. NeuroImage **31**(3) (2006) 1086–1103
13. Guo, W., Zeng, Q., Chen, Y., Liu, Y.: Using multiple tensor deflection to reconstruct white matter fiber traces with branching. In: Int. Symp. on Biomedical Imaging. (2006) 69–72
14. Zhan, W., Yang, Y.: How accurately can the diffusion profiles indicate multiple fiber orientations? A study on general fiber crossings in diffusion MRI. J. of Magnetic Resonance **183** (2006) 193–202
15. Schultz, T., Seidel, H.: Estimating crossing fibers: A tensor decomposition approach. Trans. on Visualization and Computer Graphics **14**(6) (2008) 1635–1642
16. Gössl, C., Fahrmeir, L., P utz, B., Auer, L., Auer, D.: Fiber tracking from DTI using linear state space models: Detectability of the pyramidal tract. NeuroImage **16** (2002) 378–388
17. Björnemo, M., Brun, A., Kikinis, R., Westin, C.F.: Regularized stochastic white matter tractography using diffusion tensor MRI. In: Medical Image Computing and Computer Assisted Intervention (MICCAI). (2002) 435–442
18. Zhang, F., Goodlett, C., Hancock, E., Gerig, G.: Probabilistic fiber tracking using particle filtering. In: Medical Image Computing and Computer Assisted Intervention (MICCAI). (2007) 144–152
19. Zhukov, L., Barr, A.: Oriented tensor reconstruction: Tracing neural pathways from diffusion tensor MRI. In: Visualization. (2002) 387–394
20. Poupon, C., Roche, A., Dubois, J., Mangin, J.F., Poupon, F.: Real-time MR diffusion tensor and Q-ball imaging using Kalman filtering. Medical Image Analysis **12**(5) (2008) 527–534

21. Behrens, T., Johansen-Berg, H., Jbabdi, S., Rushworth, M., Woolrich, M.: Probabilistic diffusion tractography with multiple fibre orientations: What can we gain? NeuroImage **34** (2007) 144–155
22. Julier, S., Uhlmann, J.: Unscented filtering and nonlinear estimation. IEEE **92**(3) (2004) 401–422
23. Simon, D., Simon, D.: Kalman filtering with inequality constraints for turbofan engine health estimation. IEE Proc.–Control Theory and Appl. **153**(3) (2006) 371–378
24. Frey, B., Dueck, D.: Clustering by passing messages between data points. Science **315** (2007) 972–976
25. Leemans, A., Jones, D.K.: A new approach to fully automated fiber tract clustering using affinity propagation. In: Int. Symp. on Magnetic Resonance in Medicine (ISMRM). Volume 17. 856
26. O'Donnell, L., Westin, C.F.: Automatic tractography segmentation using a high-dimensional white matter atlas. IEEE Trans. on Med. Imag. **26** (2007) 1562–75